Estimating Angle of Attack and Sideslip Under High Dynamics on Small UAVs

Article · January 2008

CITATIONS
5

READS
1,257

4 authors, including:

Rick Lind
University of Florida
150 PUBLICATIONS **1,706** CITATIONS

SEE PROFILE

Estimating Angle of Attack and Sideslip Under High Dynamics on Small UAVs

John Perry, *Geomatics Program*
Dr. Ahmed Mohamed, *School of Forest Resources and Conservation*
Baron Johnson, *Dept. of Mechanical and Aerospace Engineering*
Dr. Rick Lind, *Dept. of Mechanical and Aerospace Engineering*

406A Reed Lab, University of Florida
Gainesville, Fl 32611-0565

BIOGRAPHIES

John Perry is a graduate student in the Geomatics Program at the University of Florida. His background is in spatial measurement systems, with a research focus in developing sensor integration techniques for unmanned aerial vehicles as a platform for directly georeferenced remote sensing. E-mail: amohamed@ufl.edu

Dr. Ahmed H. Mohamed is Assistant Professor at the University of Florida - Geomatics, and Director of Navigation, Geo-referencing and Mapping (NaGeM) laboratory. He is responsible for the operation of the laboratory, for teaching and research in the field of navigation and mapping.

Baron Johnson is an aerospace engineering graduate student at the University of Florida. He has been active in UAV-related research with the Micro Air Vehicle and Flight Control Labs at UF. Baron is a licensed pilot, holding commercial, instrument, and multi-engine ratings, and is also an accomplished RC aerobatics pilot.

Dr. Rick Lind is an Associate Professor in the Department of Mechanical and Aerospace Engineering at the University of Florida. Prior to joining the faculty, he received a PhD from the University of Minnesota and spent 6 years at NASA Dryden Flight Research Center. He specializes in flight dynamics and control for novel aerospace vehicles. His work on biologically-inspired morphing aircraft has been featured on the Discovery Channel and the National Geographic Channel.

ABSTRACT

High dynamic flight is an underutilized realm of flight which has the potential to drastically expand the flight envelope and mission capability of small unmanned aerial vehicles (UAVs). The introduction of high angle of attack (*alpha*) and angle of sideslip (*beta*) flight modes to a UAV remote sensing platform would expand the mission capability of the craft by allowing for high dynamic maneuvers that orient the plane toward the observation target while maintaining trajectory control of the aircraft. Such capability would provide some compromise between the aerodynamic control of aircraft and the desire to point the sensor payload toward a desired target.

Flight control systems for small autonomous UAVs rely on real-time navigation parameters as inputs. Typically, an INS/GPS is used to solve for the six degrees of freedom motion model in the local level frame. Often, the navigation parameters are augmented using a Pitot tube to measure the air speed and tri-axial magnetometers to aid attitude estimation. On the assumption of low angle of attack and sideslip, these parameters provide adequate input to the autonomous flight control system. In order to extend the autopilot to high dynamic flight modes, however, the navigation parameters must be further augmented by measures of the angle of attack (alpha) and sideslip (beta). These additional parameters are introduced when the longitudinal axis of the air frame is non-tangential to the trajectory of the craft relative to the air mass.

This paper develops and analyzes the error associated with estimating the angles of attack and sideslip using the primary navigation parameters. The alpha and beta angles are then modeled as a zero-th order Gauss-Markov process to be augmented into the main navigation filter. The effect of the wind is also examined, as alpha and beta

angles are defined relative to the motion of the air mass. A rudimentary dynamics model for estimating a constant horizontal wind is also produced. Using the developed model, the errors associated with estimating alpha and beta angles with low-cost navigation sensors commonly used for small UAV applications is analyzed. The performance of the sensors are evaluated using data collected from a benchmarking test that emulated the expected dynamics of high dynamic flight on a small UAV.

The results show that with these readily available sensors, the alpha and beta angles can be estimated to within 4.5˚ at a confidence level of 95% with the assumption that wind is properly accounted for. Although this does not meet the desired performance goal of 2˚ at a 95% confidence interval, the available level of precision is feasible for implementation.

INTRODUCTION

Unmanned Aerial Vehicle (UAV) technology has emerged as a remote sensing platform that is highly mobile, relatively inexpensive, and safe to operate, opening up a huge potential for expanding the scope and availability of remote sensing data at biologically relevant scales [Pearlstine et. al. 2001]. Significant advantages of small UAVs in the 10 kg range are their ease of transport and hand-launching capability [Watts et. al., 2008]. In order to meet the size and weight goals of these aircraft, it is necessary to minimize the size and complexity of the remote sensing payload. To this end, it is desirable to use a strapdown approach where the imaging system and navigation components are rigidly fixed to the aircraft frame. This avoids the cost, weight, and complexity of a gimbaled payload system or a morphing airframe [Grant et. al., 2006]. A strapped down payload introduces a significant challenge on an aerial platform, however, because orienting the sensor toward the target can only be accomplished by reorienting the plane. In a dynamic flight environment, this can be at odds with the needs of the autonomous flight control system to maintain course and conduct flight maneuvers.

It is pertinent to distinguish the relevant modes of flight in order to highlight the particular control and navigation needs of each. In normal flight, lift is primarily generated by the wing surfaces moving through the air mass. The aircraft's angle of attack is below critical alpha, and therefore the linearized equations of motion for this flight regime apply [Klein & Morelli, 2006]. In this flight regime, angle of attack measurements are not usually required for basic navigation and control solutions and are rarely computed in conventional autopilot flight control systems. Small variations in the angle of attack are negligible, and for this reason the angle of attack is not usually measured or calculated as an independent input to the autopilot flight control system. In high alpha flight, the aircraft is held at an angle of attack beyond the critical angle of attack at which stall occurs. Within this mode, lift is generated by both the relative motion of the wing to the air mass as well as directly by the propulsion. As the angle of attack continues to increase toward 90˚, the lift generated by the wings becomes negligible relative to direct propulsion, and at this point the craft is said to be in hover [Klein & Morelli, 2006]. This paper focuses on the high alpha flight regime between normal flight and hover.

Controlled high angle of attack flight is facilitated by three factors. First, the high thrust-to-weight ratio typical of many small UAVs provides a significant contribution to the vertical lift force when in high alpha flight. Second, a tractor-type propulsion system with a nose-mounted propeller provides airflow over the control surfaces despite relatively low forward velocity. Third, large control surfaces with large ranges of motion, particularly elevators, provide the necessary control forces when operating primarily in the propwash. It has been well demonstrated that UAVs are capable of maneuvering in a hovering mode of flight [Johnson et. al., 2006]. As a result, it is clear that the propulsion is great enough to sustain a high angle of attack mode on many small UAV platforms. Furthermore, human-controlled R/C aircraft of similar size are routinely flown in high angle of attack modes during acrobatic competition, thus demonstrating the sufficiency of the control surfaces for our purpose.

Three relevant maneuvers will be discussed to illustrate the capabilities of high dynamic flight modes. In general, high dynamic modes allow for slower speeds, tighter turns, and the ability to maintain horizontal attitudes during turning maneuvers. Some maneuvers which would be applicable to the UAV as a remote sensing platform include:

- High Angle of Attack
  - Maintain level attitude at reduced speed
  - Perform short-field landings by decreasing approach speed and increasing approach angle
  - Navigate tightly constrained airspaces such as urban environments
  - Capture oblique photographs about the pitch axis
- High Angle of Sideslip
  - Maintain a level attitude while turning, optimizing route planning for vertical photographs
  - Capture oblique photographs about the roll axis

Figure 1. Typical aerobatic UAV design conducting a high alpha flight maneuver

The advantages are practically illustrated in the need for taking vertical photographs. Vertical photographs, where the imaging sensor is oriented downward along the gravity vector, are an ideal source for orthophoto maps. To accomplish this using a strapdown sensor package, the plane must fly as close as possible to level. However, typical flight control systems will maneuver the plane horizontally by inducing roll in a banking turn that will tilt the photograph, rendering the data less useful if not useless. This situation restricts the flight regime for data collection to straight and level flight. This can be impossible in spatially restricted urban environments. Even in clear airspace, this limitation will require additional flight planning and wasted flight time to allow for turning maneuvers outside of the target area. A direct solution to this would be to perform horizontal, non-banking turns by inducing a high angle of sideslip.

Significant drawbacks to these high dynamic flight modes include increasing the complexity of the control system for autonomous applications and the susceptibility to undesirable flight dynamics [Bauer et. al., 1997]. As mentioned previously, linearized aircraft equations of motion are non-applicable in high dynamic regimes. As a result, the autopilot control system within these flight modes must be augmented. Furthermore, even within the high alpha flight mode, small variations in the angle of attack and sideslip can lead to drastically different dynamics. For example, the NASA X-29 project demonstrated that an uncommanded roll oscillation that was prevalent in high angle of attack flight could be controlled by the introduction of as little as 1-2 degrees of sideslip [Iliff & Wang, 1997]. This kind of resolution on the alpha and beta parameters are of primary interest to this paper, as any control system development is predicated on the accurate estimation and providence of the parameters. As a result, the goal of this paper is to characterize a navigation solution that can provide alpha and beta estimates within 2 degrees at a 95% confidence level.

DEFINITIONS

Angle of Attack is defined as the angle measured between the longitudinal axis of the airframe and the relative motion of the air, measured along the Y-Z plane of the body frame, mathematically given as

$$\alpha = \operatorname{atan}\left(\frac{v_z}{v_y}\right) \quad \textbf{(1)}$$ [Yechout et. al., 2003].

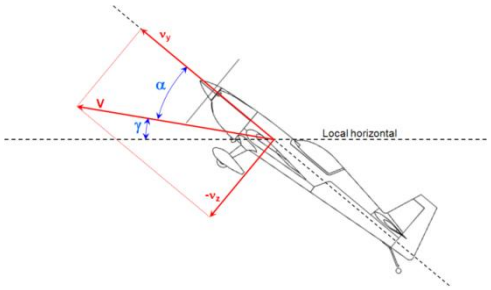

Figure 2. Angle of attack, α.

Angle of Sideslip is defined as the angle measured between the longitudinal axis of the airframe and the relative motion of the air, measured along the Y-X plane of the body frame, mathematically given as

$$\beta = \operatorname{atan}\left(\frac{v_x}{v_y}\right) \quad \textbf{(2)}$$ [Yechout et. al., 2003].

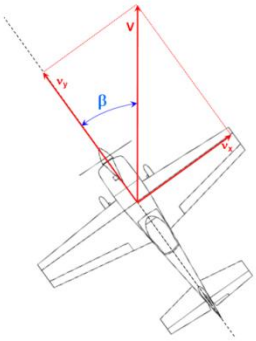

Figure 3. Angle of sideslip, β.

Where, in both of these definitions v denotes the relative motion of the airframe through the air mass defined in the body frame. It should be noted that the proper definition of angle of sideslip involves all three body frame velocity components and represents a 3-dimensional angle [Yechout et. al., 2003]. However, when dealing with high angle of attack flight situations, this definition creates significant coupling between alpha and beta and can introduce ambiguity. Therefore, for the purpose of this research, the 2-dimensional definition of beta was used to maintain independence between alpha and beta.

THE WIND FACTOR

It is critical to note that the definition of the alpha and beta angles explicitly defines the motion relative to the *air mass*. In practical terms, this means that the wind must be taken into account. Therefore, we must modify the velocities usually provided in the inertial navigation solution to include the wind velocity vector. This is most conveniently accomplished in the local-level frame, such that

(3)

$$\begin{bmatrix} v_x^{air} \\ v_y^{air} \\ v_z^{air} \end{bmatrix} = \begin{bmatrix} v_x^{l} \\ v_y^{l} \\ v_z^{l} \end{bmatrix} - \begin{bmatrix} v_x^{wind} \\ v_y^{wind} \\ v_z^{wind} \end{bmatrix}$$

where $v^{air}$is the velocity of the craft relative to the air mass defined in the local level frame, v^l is the inertial velocity of the craft defined in the local level frame, and v^{wind} is the velocity of the wind defined in the local level frame.

A common assumption made in short-duration UAV flights is that of a constant, horizontal wind. We will use this definition to develop a rudimentary method for observing the wind vector. Most small UAVs include an air speed sensor, usually a Pitot tube, which measures the speed of the craft along the longitudinal axis of the craft relative to the air mass. Given the further assumption that these observations are made when the craft is flying horizontally, we have

(4)

$$A = \sqrt{(V\sin\psi - W\sin\theta)^2 + (V\cos\psi - W\cos\theta)^2}$$

where A is the air speed as measured by the Pitot tube, V is the inertial speed of the craft measured in the local level, ψ is the heading of the craft, W is the speed of the constant and horizontal wind, and θ is the heading of the wind.

Knowing that we can measure the inertial speed and the heading of the craft using the inertial navigation system, and can measure the air speed using the Pitot tube, we can differentiate with respect to our unknowns, wind speed and direction, to give

(5) $F = A^2$

(6) $\frac{\partial \mathrm{F}}{\partial \theta} = \frac{-\mathrm{WV}}{\mathrm{A}}\sin(\psi - \theta)$

(7) $\frac{\partial \mathrm{F}}{\partial W} = \frac{1}{\mathrm{A}}(\mathrm{W} - \mathrm{V}\cos(\psi - \theta))$

These equations can then be used to solve for the wind speed and direction using a real-time Kalman filter. The model presented here is highly simplified and has not been verified experimentally for accuracy. A more complete apparatus and method for measuring the wind vector can be found in [Kroonenberg et. al., 2008].

It is evident that the wind will affect velocity measurements required to calculate the angle of attack and sideslip. This paper develops an error analysis which relies on the assumption of zero wind. In this case, the velocity relative to the air mass is equal to the inertial velocity of the craft. To account for the wind in the error analysis, the following straightforward rules will apply. First, the inertial velocities must be modified with the wind vector velocities, as in Eqn. 1. Second, the variance of the velocity measurements used in the error analysis will be changed so that

(8) $\sigma_v = \sqrt{\sigma_v^{inertial\,2} + \sigma_v^{wind\,2}}$

All other developments remain the same. As we shall see, it is primarily the magnitude and ratio of the velocity components which affect the error in the alpha and beta estimates. Under a constant horizontal wind, the ratio of these components will be unaffected by the wind. Therefore, it is when the magnitude of the wind is large relative to the speed of the craft that is of most practical concern.

ERROR ANALYSIS

Using the definitions for alpha and beta angles and the general law of error of propogation of variances, the variances for their calculated values are, respectively,

(9)

$$\sigma_\alpha{}^2 = \sigma_{v_y^b}{}^2\left(\frac{\partial\alpha}{\partial v_y^b}\right)^2 + \sigma_{v_z^b}{}^2\left(\frac{\partial\alpha}{\partial v_z^b}\right)^2 + 2\mathrm{cov}\left(v_y^b, v_z^b\right)\left(\frac{\partial\alpha}{\partial v_z^b}\right)\left(\frac{\partial\alpha}{\partial v_y^b}\right)$$

(10)

$$\sigma_\beta{}^2 = \sigma_{v_y^b}{}^2\left(\frac{\partial\alpha}{\partial v_y^b}\right)^2 + \sigma_{v_x^b}{}^2\left(\frac{\partial\alpha}{\partial v_x^b}\right)^2 + 2\mathrm{cov}\left(v_y^b, v_x^b\right)\left(\frac{\partial\alpha}{\partial v_x^b}\right)\left(\frac{\partial\alpha}{\partial v_y^b}\right)$$

[Ghialini & Wolf, 2006]

On the assumption that the covariance between velocity measurements is small, this is simplified and expanded to

$$\textbf{(11)} \qquad \sigma_\alpha{}^2 = \sigma_{v_y^b}{}^2 \left(\frac{v_z^b}{v_y^{b2}+v_z^{b2}}\right)^2 + \sigma_{v_z^b}{}^2 \left(\frac{v_y^b}{v_y^{b2}+v_z^{b2}}\right)^2$$

$$\textbf{(12)} \qquad \sigma_\beta{}^2 = \sigma_{v_y^b}{}^2 \left(\frac{v_x^b}{v_y^{b2}+v_x^{b2}}\right)^2 + \sigma_{v_x^b}{}^2 \left(\frac{v_y^b}{v_y^{b2}+v_x^{b2}}\right)^2$$

Further simplification gives,

$$\textbf{(13)} \qquad \sigma_\alpha{}^2 = \left(\frac{1}{\frac{v_y^b}{v_z^b}+\frac{v_z^b}{v_y^b}}\right)^2 \left[\left(\frac{\sigma_{v_y^b}}{v_y^b}\right)^2 + \left(\frac{\sigma_{v_z^b}}{v_z^b}\right)^2\right]$$

$$\textbf{(14)} \qquad \sigma_\beta{}^2 = \left(\frac{1}{\frac{v_y^b}{v_x^b}+\frac{v_x^b}{v_y^b}}\right)^2 \left[\left(\frac{\sigma_{v_y^b}}{v_y^b}\right)^2 + \left(\frac{\sigma_{v_x^b}}{v_x^b}\right)^2\right]$$

From this, it is evident that the primary factors in the error propogation are the ratios and magnitudes of the relevant velocity components. Holding all other factors equal, it is clear that for both the alpha and beta angles, the error is maximized when the ratios $\frac{v_y^b}{v_z^b}$ and $\frac{v_y^b}{v_x^b}$, respectively, are at unity, as shown in figure 3.

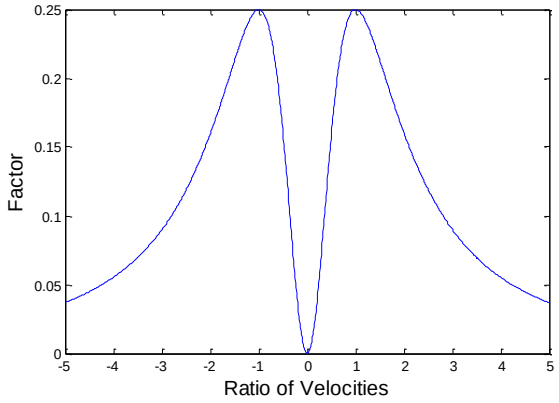

Figure 4. Plot of $\left(\frac{1}{\frac{v_y^b}{v_z^b}+\frac{v_z^b}{v_y^b}}\right)^2$ showing the contribution of the ratio of velocities.

However, the most significant factor is the magnitude of the individual velocity components. For each velocity axis, the error propogation function is unbounded as the velocity along both axes falls to zero. Importantly, it is only when both relevant velocity components approach zero. The factor resulting from the ratio of velocities prevents the error from being exponential as long as at least one of the velocities remains relatively large. The exponential growth in the variance resulting from low velocity is of serious concern to the proposal for controlling the aircraft using the angle of attack and sideslip. This is an important point and will be considered in the subsequent discussion. The effect is clear when plotting the value of the variances over the normal velocity range of a small UAV and with the expected variances in velocity measurement using low-cost MEMS IMU's and code solution GPS, as in figures 4 and 5.

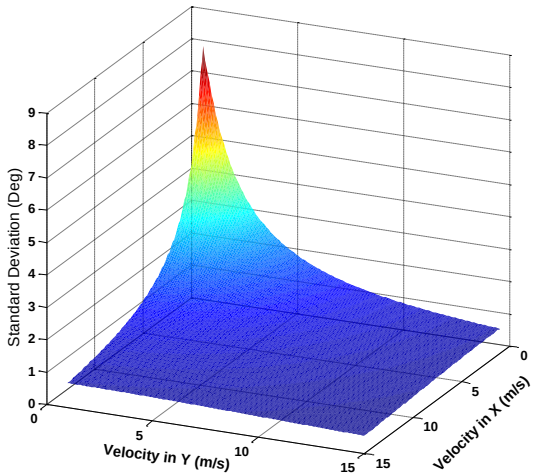

Figure 5. The standard deviation of the angle of sideslip measurement with a standard deviation of .2 m/s and magnitude of 1-15 m/s along each body velocity component.

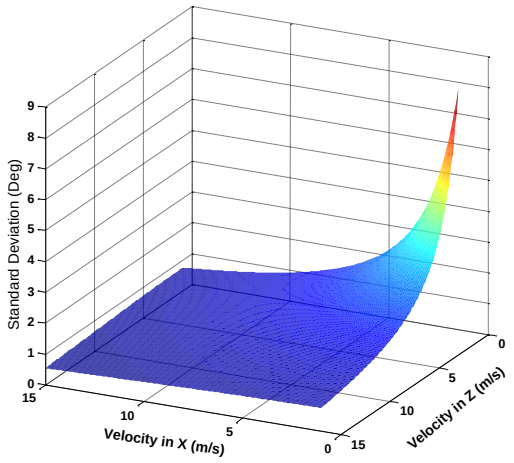

Figure 6. The standard deviation of the angle of attack measurement with a standard deviation of .2 m/s and magnitude of 1-15 m/s along each body velocity component.

As shown in these figures, the error grows rapidly as the plane's velocity falls to zero. It should be noted, however, that in laying out the desired high dynamic flight modes we clearly distinguished it from hover mode. Based on the fact that the desired flight mode would maintain a considerable contribution to lift from the wind moving over the wings, the velocity components relative to the air mass must be significant. As the velocity falls and the plane transitions into a hovering flight mode, the angle of attack and sideslip become less relevant to the control loop. This prompts the question, then, of the minimum air speed of the aircraft that should be targeted when flying in high dynamics. This investigation lies in future work, as will be discussed, and for now an arbitrary airspeed of 5 m/s with a minimum of 1 m/s along any individual axis will be used for analysis.

From the criteria of a minimum airspeed of 5 m/s and minimum component velocity of 1 m/s, the minimum required accuracy of the navigation parameters can be calculated. To simplify the analysis, the assumption is made that the precision of velocity measurements along the three body axes are approximately equal, that is

(15) $$\sigma_{v_x^b} \cong \sigma_{v_y^b} \cong \sigma_{v_z^b}$$

In order to meet the desired precision of two degrees in either the alpha or beta angles at a 95% confidence level, this gives a standard deviation of body-frame velocities measurements of approximately 0.1 m/s.

ALGORITHM DEVELOPMENT

It is in the interest of this paper to develop a practical method of estimating the alpha and beta angles for use as in-flight feedback inputs to the autopilot control loop. As the necessary variables are already available within the Kalman filter that is running to provide navigation parameters, it is a logical step to augment the existing navigation filter with these additional parameters. In order to do so, an adequate model of the alpha and beta dynamics must be developed. We do so by modeling the parameters as a zero-th order Gauss Markov process, such that

(16) $$\delta\dot{\alpha} = w_\alpha$$

(17) $$\delta\dot{\beta} = w_\beta$$

where w_α and w_β are Gaussian white noise [Gelb, 1974]. In this manner, the estimates for the angle of attack and sideslip may be generated. In addition, statistical information extracted from the filter may be used to aid in the transition periods where the alpha and beta angles become unstable. Empirical data may be used to extract refined estimates for the a priori variances of the estimates. Furthermore, this model can be extended to a first-order Gauss-Markov model given sufficient empirical data from which to extract spectral densities.

EXPERIMENTAL RESULTS

Having developed the necessary error analysis, tests were conducted to determine the ability of commercial off-the-shelf components suitable for use on small UAV applications to meet the performance goals. To this end, a MEMSENSE nIMU, a 6 DoF MEMS-based IMU was selected [Memsense, 2008]. This was paired with an EagleTree systems GPS that provides a standard code solution single-frequency GPS position. As a check for accuracy, a Novatel SPAN system was used, with a 1˚/hr HG1700-AG11 IMU and a post-processed dual-frequency differential GPS solution [Novatel, 2008].

MEMSENSE nIMU [Memsense, 2008]		
	Gyros	**Accelerometers**
Dynamic Range	±600˚/s	±5G
Sensitivity	0.0183˚/s	$1.526e^{-4}$ G
Drift	±1˚/s	±30mG
Noise	.56˚/s	4.87mG

The tests were conducted so as to simulate expected flight dynamics, with a speed of around 15 m/s and alpha and beta angles varying from 0 to 45˚. A circular track, depicted in Figure 7 was used, and the sensors were mounted on a free-moving platform on a ground vehicle. The solution was processed using Waypoint Inertial Explorer software, and the alignment for the low-accuracy system was transferred from the Novatel SPAN system.

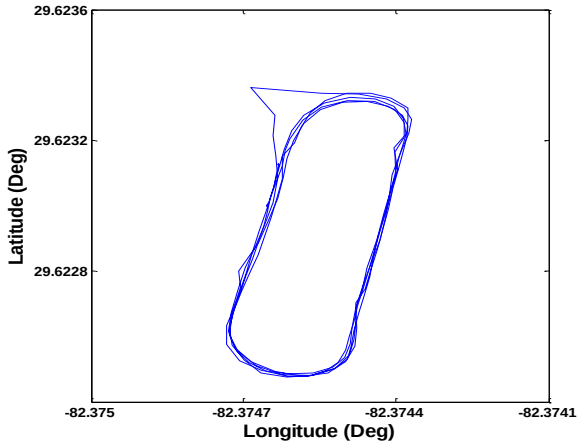

Figure 7. Horizontal trajectory of the vehicle during data collection.

The GPS track illustrated in Figure 7 shows the effect of a brief period of poor quality solutions during a turn in the northwest corner of the track. Statistical estimates of the

navigation parameter errors are presented in Figures 8 and 9. Standard deviation of velocities along the East, North, and Up directions were approximately 0.2 m/s during dynamic conditions.

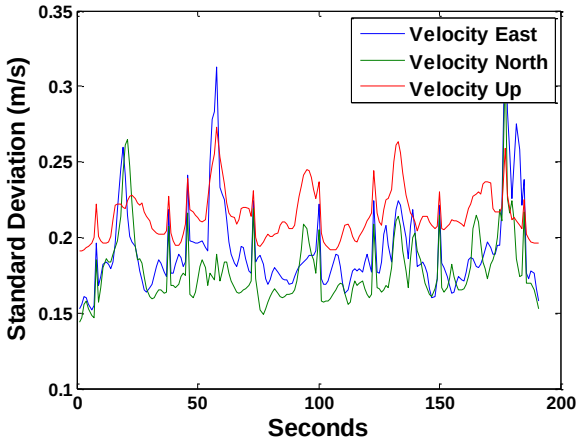

Figure 8. Standard deviation of the velocity components in the local-level frame.

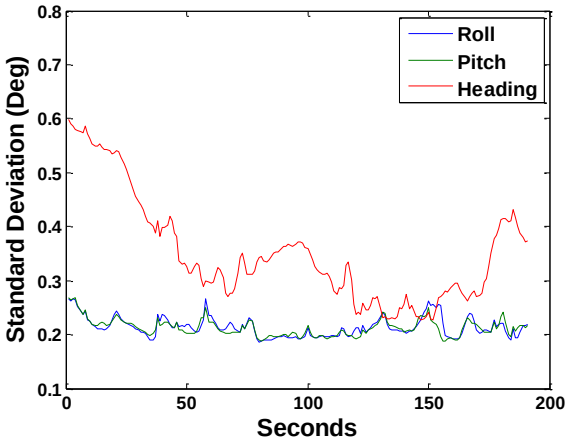

Figure 9. Standard deviation of the attitude components in the local-level frame.

The standard deviation of the roll and pitch measurements during dynamic testing were 0.2˚ and the heading was slightly worse at 0.35˚, as expected. These variances resulted in an average standard deviation of 0.8˚ for the angle of attack estimate and 0.4˚ for the sideslip estimate under dynamics. As can be noted from figure 10, the additional parameters were highly unstable during the static portion of the test. This verifies, in part, the developed error propogation model. Figure 11 windows the data set to only the dynamic portion of the flight test. The periodic spikes in the accuracy of the angle of attack solution correspond to slower velocities incurred during turning maneuvers.

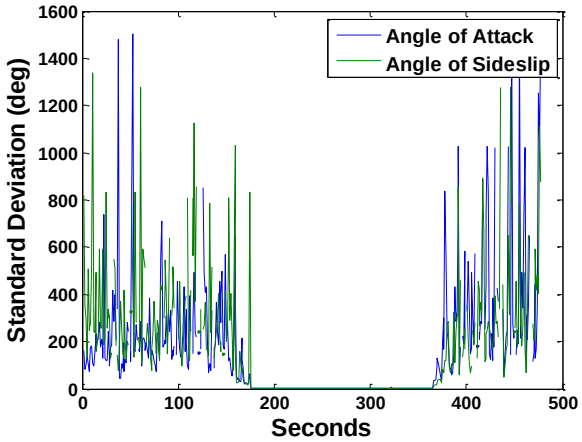

Figure 10. Standard deviation of the angle of attack and sideslip over the entire data collection period.

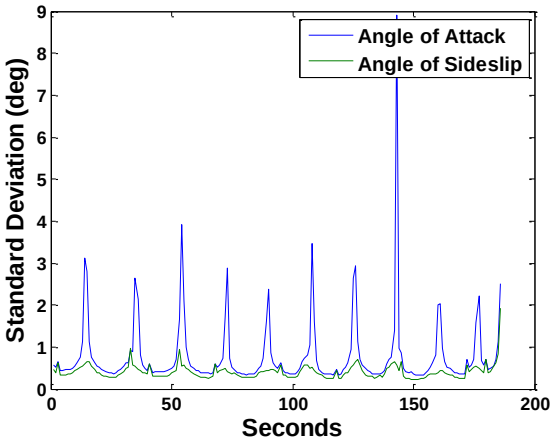

Figure 11. Standard deviation of the angle of attack and sideslip during the dynamic portion of the test.

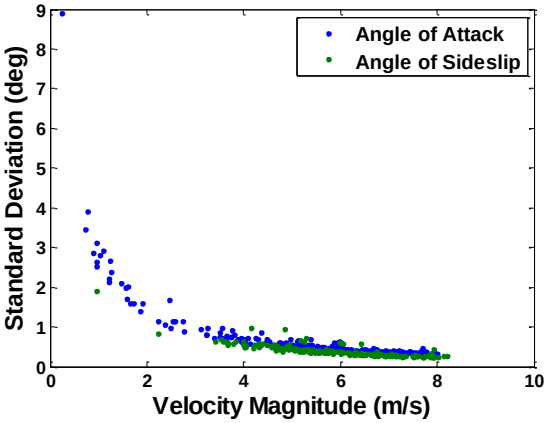

Figure 12. Standard deviation of the angle of attack and sideslip versus the magnitude of the component velocities on a linear scale.

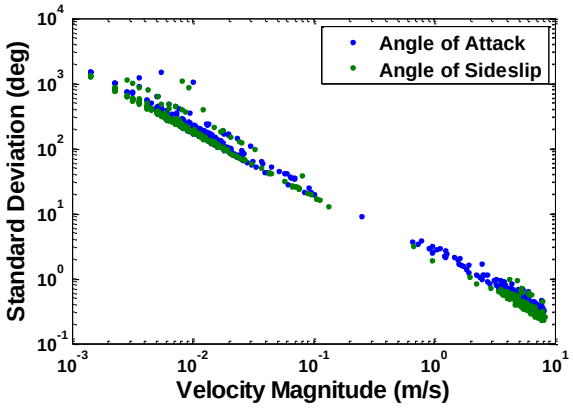

Figure 13. Standard deviation of the angle of attack and sideslip versus the magnitude of the component velocities on a logarithmic scale.

Figures 12 and 13 show the standard deviation in the angle of attack plotted against the total velocity of the sensors, plotted on both linear and logarithmic scales. This demonstrates the developed model for exponential growth in error as the combined velocities along the relevant axes go to zero.

CONCLUSION

Based on the developed error model and the experimental results concerning the precision of commercial off-the-shelf navigation components, the alpha and beta angles can be estimated to within 1.6˚ and 0.8˚, respectively, at a confidence level of 95%. However, these figures are based on an experiment in which the average speed was above the minimum criteria developed for a robust estimation that operates through the dynamic transition between high alpha and hover flight. The experimentally observed variances would give a precision of about 4.5˚ for alpha and beta angles using the minimum velocity criteria. Although this does not meet the performance goal of 2˚ desired as a robust input to an autopilot control loop for high dynamic flight, it is still a feasible proposition. More accurate navigation components would undoubtedly increase the accuracy, and the difference in precision desired is less than an order of magnitude, suggesting evolutionary developments in MEMS sensors will close this gap.

FUTURE WORK

Further work and experimental validation is required of the algorithm used for wind estimation, a critical component of defining the velocities relative to the air mass. Alternatively, wind data collected by airports and other meteorological sources could be used to provide estimates at flight time.

The Kalman filter developed for the alpha and beta estimation has also not been validated experimentally. Flight data collected during high dynamic flight needs to be analyzed and applied to tune the proposed Kalman filter's performance. This will provide a necessary baseline processing algorithm that will allow proper benchmarking of estimated versus 'true' alpha and beta angles.

ACKNOWLEDGEMENTS

Thanks are owed to the effort of Damon Wolfe, a recent graduate of the University of Florida Geomatics Program, who assisted in preparing for and conducting the data collection.

REFERENCES

Bauer, J., Clarke, R., and Burken, J., (1995). "Flight Test of the X-29A at High Angle of Attack: Flight Dynamics and Controls," National Aeronautics and Space Administration, Dryden Flight Research Center, Edwards, CA.

Frank, A., McGrew, J., Valenti, M., Levine, D., and How, J. (2007) "Hover, Transition, and Level Flight Control Design for a Single-Propeller Indoor Airplane," AIAA Guidance, Navigation and Control Conference and Exhibit, Hilton Head, SC, Aug. 20-23.

Gelb., A. (1974) Applied Optimal Estimation. The M.I.T. Press, Cambridge, MA.

Ghiliani, C., and Wolf., P. (2006) Adjustment Computations: Spatial Data Analysis 4th Edition. Wiley & Sons, Inc., Hoboken, NJ.

Grant, D., Abdulrahim, M., and Lind, R. (2007) "Flight Dynamics of a Morphing Aircraft Utilizing Multiple-Joint Wing Sweep," AIAA Atmospheric Flight Mechanics Conference and Exhibit, Keystone, Colorado, Aug. 21-24.

Gree, W., and Oh, P. (2006) "Autonomous Hovering of a Fixed-Wing Micro Air Vehicle," Proceedings of the 2006 IEEE International Conference on Robotics and Automation, Orlando, FL.

Iliff, K., and Wang, K. (1997) "Flight Determined Subsonic Longitudinal Stability and Control Derivatives of the F-18 High Angle of Attack Research Vehicle (HARV) With Thrust Vectoring," National Aeronautics and Space Administration, Dryden Flight Research Center, Edwards, CA.

Johnson, E., Turbe, M., Wu, A., Kannan, S., and Neidhoefer, J. (2006) "Flight Test Results of Autonomous Fixed-Wing UAV Transitions to and from Stationary Hover," AIAA Guidance, Navigation, and Control Conference and Exhibit, Keystone, CO, Aug. 21-24.

Klein, V., and Morelli, E. (2006) Aircraft System Identification, Theory and Practice, AIAA Education Series, AIAA, Reston, VA.

Memsense, Inc. (2008). nIMU Datasheet v2.11., http://www.memsense.com/images/downloads/65/Datasheet-v2.11.pdf

Mueller, T. and DeLaurier, J. (2008) Aerodynamics of Small Vehicles. Annual Review of Fluid Mechanics. Vol. 35, pp. 89–111.

Novatel, Inc. (2008). SPAN Technology Product Sheet, http://www.novatel.com/Documents/Papers/SPAN.pdf

Pearlstine, L., Percival, F., Carthy, R., Abd-Elrahman, A., Morris, S. (2001). Development of a Practical Unmanned Aerial Vehicle for Natural Resource Sampling. Proceedings of the 18th Biennial ASPRS Workshop on Color Photography & Videography in Resource Assessment

Van den Kroonenberg, A., Spieß, T., and Bange, J. (2008) First wind measurements with the Meteorological UAV 'M2AV Carolo'. 18th Symposium on Boundary Layers and Turbulence. June 10.

Watts, Adam, Bowman, W., Abd-Elrahman, A, Mohamed, A, Perry, J, Kaddoura, Y, and Lee, K (2008), "Unmanned Aircraft Systems (UASs) for ecological research and natural-resource monitoring", Journal of Ecological Restoration, Vol. 26 , No. 1.

Wright, K. and Lind, R. (2007) "Investigating Sensor Emplacement on Vertical Surfaces for a Biologically-Inspired Morphing Design from Bats," AIAA Atmospheric Flight Mechanics Conference and Exhibit, Hilton Head, SC, Aug. 20-23.

Yechout, T., Morris, S., Bossert, D., and Hallgren, W. (2003) Introduction to Aircraft Flight Mechanics: Performance, Static Stability, Dynamic Stability, and Classical Feedback Control. American Institute of Aeronautics and Astronautics, Inc., Reston, VA.